

Distance-Aware BeamSpace Modulation for Near-Field Spectral Efficiency Improvement

Kaiqian Qu, Ke Pang, Hui Zhao, Ahmed Elzanaty, *Senior Member, IEEE*, and Shuaishuai Guo, *Senior Member, IEEE*

Abstract—In the near-field region of extremely large-scale multiple-input multiple-output (XL-MIMO), the spatial degrees of freedom (DoFs) increase sharply. BeamSpace modulation (BM) is an effective scheme for leveraging the massive DoFs of XL-MIMO with a small number of radio frequency (RF) chains. This letter proposes a distance-aware BM (DABM) strategy to achieve greater spectral efficiency (SE) improvement. By introducing selection switches, the number of activated RF chains is dynamically adjusted based on distance-related DoFs. Then, we derive a concise upper bound for the SE of BM. Based on this, we derive the optimal number of RF chains to reach the maximum SE improvement at different spatial DoFs. Finally, simulation results demonstrate that DABM effectively adapts to varying DoFs at different distances, thereby enhancing SE.

Index Terms—BeamSpace modulation, distance-aware, XL-MIMO, near-field communications, spectral efficiency

I. INTRODUCTION

AS a key technology for 6G, the extremely large-scale multiple-input multiple-output (XL-MIMO) is expected to achieve a tenfold increase in spectral efficiency compared to the massive multiple-input multiple-output (MIMO) in 5G [1], [2]. The expansion of array size leads to the near-field dominance, and the near-field communication has become a focal point of significant attention [3]–[5].

Due to the distance dimension introduced by near-field spherical waves, many advantages are brought to near-field communications. For example, near-field can achieve beam focusing, concentrating energy at a specific position rather than in a certain angular direction. Therefore, Wu et al. proposed the concept of LDMA, which allows more users to access and achieves higher spectral efficiency (SE) compared to space-division multiple access [4]. Similarly, [5] verified that the near-field provides new degrees of freedom (DoFs) for multi-user interference management.

Moreover, in XL-MIMO, the spherical waves reduces the correlation between different transmit-receive antenna pairs,

The work is supported in part by the National Natural Science Foundation of China under Grant 62171262; in part by Shandong Provincial Natural Science Foundation under Grant ZR2021YQ47; in part by the Taishan Young Scholar under Grant tsqn201909043. (*Corresponding author: Shuaishuai Guo).

Kaiqian Qu and Shuaishuai Guo are with School of Control Science and Engineering, Shandong University, Jinan 250061, China (e-mail: qukaiqian@mail.sdu.edu.cn, shuaishuai_guo@sdu.edu.cn).

Ke Pang is with the School of Microelectronics and Control Engineering, Changzhou University, Changzhou 213164, China (e-mail: pangke@cczu.edu.cn).

Hui Zhao is with the Communication Systems Department, EURECOM, 06410 Sophia Antipolis, France (e-mail: hui.zhao@eurecom.fr).

Ahmed Elzanaty is with the 5GIC & 6GIC, Institute for Communication Systems (ICS), University of Surrey, Guildford, GU2 7XH, United Kingdom (e-mail: a.elzanaty@surrey.ac.uk)

significantly enhancing the spatial DoFs [3], [6]. Furthermore, the DoFs increase as the communication distance decreases. This indicates a significantly increased multiplexing gain compared to the far-field line-of-sight (LoS) channel. The work [7] proposed hybrid precoding with a limited number of radio frequency (RF) chains to utilize the DoFs. Reference [8] proposed a distance-aware precoding (DAP) structure with a variable number of activated RF chains that can adapt to the large number of DoFs changing with distance. However, this also means that [7] and [8] assume a sufficient number of RF chains to match the available DoFs. Unlike [7] and [8], our prior work [9] introduced beamSpace modulation (BM) into XL-MIMO, which utilizes beamSpace selection to enhance capacity with a limited and fixed number of RF chains. Nevertheless, the specific impact of the number of RF chains on the performance of BM has not been studied. In the near-field, the number of DoFs changes dynamically with distance. How many RF chains are needed to maximize the performance gains of BM, and can BM maintain optimal gains under dynamically changing distances?

In this letter, we propose a novel distance-aware BM (DABM) scheme where the number of activated RF chains is dynamically adjusted according to the distance-related DoFs. We analyze the SE of BM and then optimize the number of activated RF chains in DABM. For that, we derive an approximate closed-form solution to obtain the optimal number of activated RF chains in DABM to achieve the maximum SE improvement over different distances. Simulation results validate the effectiveness of DABM in further enhancing system SE.

II. SYSTEM MODEL

In the XL-MIMO system, the numbers of transmitting and receiving antennas are denoted as N_t and N_r , respectively. The transmitter are equipped with N_{RF}^T RF chains. For simplicity, we assume that an optimal digital combiner is employed at the receiver side. To guarantee the full spatial multiplexing gain, the number of data streams N_s is equal to N_{RF}^T .

A. Channel Model

The near-field LoS channel model is considered in this letter, which adheres to the assumptions of the geometric

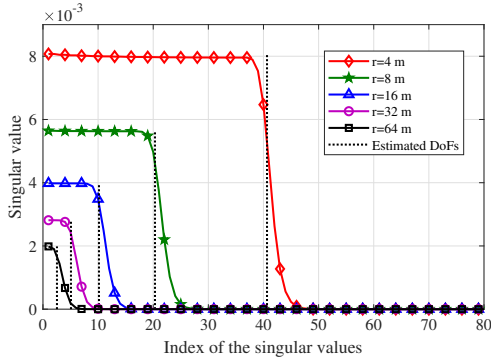


Fig. 1. Singular values and DoFs for a pair of parallel 256-antenna ULAs at 30 GHz, r is the distance between the transceiver.

free-space propagation [10], [11]. The (m, n) -th element of complex channel \mathbf{H} can be modeled as¹ [8]–[11]

$$h_{m,n} = \frac{\lambda}{4\pi r_{m,n}} e^{-j\frac{2\pi}{\lambda} r_{m,n}}, \quad (1)$$

where $r_{m,n}$ represents the distance between the n -th transmitting antenna and the m -th receiving antenna, and λ stands for the wavelength of the carrier wave.

Fig. 1 illustrates the singular values of channels (in the reverse order). Specifically, we consider the transceivers as a pair of parallel 256-antenna uniform linear arrays (ULAs) operating at 30 GHz, with an inter-antenna spacing of half a wavelength. It is shown that the singular values fall off very slowly until they reach a critical point, after which they drop sharply. The critical value reflects the effective number of spatial DoFs. Such a behavior is well known for the eigenvalues of problems of the prolate spheroidal wave functions (PSWFs) [12].

For the eigenvalues of PSWFs, the breaking point value can be calculated as $\frac{D_t D_r}{\lambda r}$, where D_t (D_r) is the array aperture at the transmitter (receiver) and r is the transmitter-receiver distance [Eq. (67), 12]. Importantly, it has been demonstrated in [8], [12] using Green’s function that the singular values of the near-field LoS channel under ideal continuous aperture can be approximated by the eigenvalues of the PSWFs. Therefore, the estimated number of DoFs can be expressed as $N_{\text{DoF}} \approx \frac{(N_t - 1)(N_r - 1)d^2}{\lambda r}$. And the first N_{DoF} singular values that decrease slowly can be considered approximately identical according to the properties of PSWFs. The dashed line in the figure illustrates the estimated number of DoFs, validating the above discussion. Furthermore, the number of DoFs increases as the communication distance r decreases. Assuming the near-field DoF threshold is set to $\Delta = 3$, the near-field distance under the simulation settings of Fig. 1 can be calculated as $R_N \approx \frac{(N_t - 1)(N_r - 1)d^2}{\lambda \Delta} \approx 54$ m [13].

B. BeamSpace Modulation

In a traditional spatial multiplexing system, data symbol vectors are transmitted by right singular vectors corresponding

¹Due to the severe path loss effect in mmWave/Thz frequency, the channel gains of the non-LoS path are negligible compared to that of LoS paths.

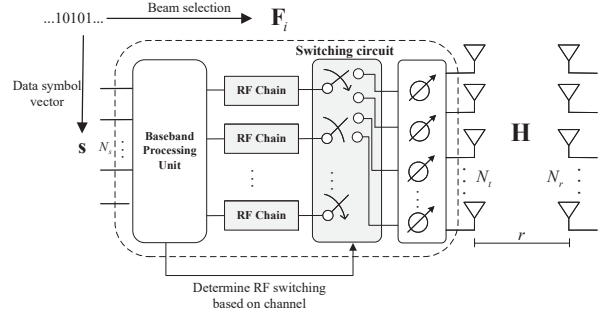


Fig. 2. System model of a DABM-based XL-MIMO communications system.

to the N_{RF}^T largest singular values. In contrast, BM selects N_{RF}^T vectors from N_{DoF} right singular vectors to form a beamformer \mathbf{F}_i for data transmission, where N_{DoF} is the number of non-zero singular values of the channel. There exist a total of $K = \binom{N_{\text{DoF}}}{N_{\text{RF}}^T}$ beamformer candidates. Therefore, activating different beamformers can convey additional information. As illustrated in Fig. 2, the input information bits are split into two parts to select the data symbol vector $\mathbf{s} \in \mathbb{C}^{N_s}$ and beamformer $\mathbf{F}_i \in \mathbb{C}^{N_t \times N_{\text{RF}}^T}$. Let $\mathcal{F} = \{\mathbf{F}_1, \mathbf{F}_2, \dots, \mathbf{F}_K\}$ represents the beamformer set². The received signal vector is of the form

$$\mathbf{y} = \mathbf{H}\mathbf{F}_i\mathbf{s} + \mathbf{n}, \quad (2)$$

where \mathbf{n} is the complex Gaussian noise with zero mean and covariance $\sigma_n^2 \mathbf{I}_{N_r}$.

III. DISTANCE-AWARE BEAMSPACE MODULATION

The beamformer set \mathcal{F} related to N_{RF}^T and N_{DoF} affects the performance of BM. In this section, we design the DABM scheme and analyze the impact of N_{RF}^T on the SE of BM. The selection switches are utilized to flexibly activate RF chains as shown in Fig. 2.

A. SE Analysis of BM

According to Theorem 1 in [14], the symbol vector \mathbf{s} with zero-mean Gaussian is fed into the precoder \mathbf{F}_i , resulting in the received vector \mathbf{y} following the distribution of the complex Gaussian mixture model (GMM). Then, the probability density function (PDF) of \mathbf{y} is expressed as

$$f(\mathbf{y}) = \sum_{i=1}^K p_i f_i(\mathbf{y}), \quad (3)$$

where p_i is the activation probability of \mathbf{F}_i and satisfies $\sum_{i=1}^K p_i = 1$. In Eq. (3), $f_i(\mathbf{y})$ is the PDF of complex Gaussian distribution, taking the form

$$f_i(\mathbf{y}) = P(\mathbf{y}|\mathbf{F} = \mathbf{F}_i) = \frac{1}{\pi^{N_r} \det(\Sigma_i)} \exp(-\mathbf{y}^H \Sigma_i^{-1} \mathbf{y}), \quad (4)$$

with $\Sigma_i = \mathbf{I}_{N_r} + \frac{1}{N_{\text{RF}}^T \sigma_n^2} \mathbf{H}\mathbf{F}_i\mathbf{F}_i^H \mathbf{H}^H$.

Remark 1: We assume that power allocation among different data streams for any \mathbf{F}_i follows the water-filling algorithm,

²BM is not dependent on a specific codebook; other codebooks applicable to XL-MIMO can also be used for BM.

which depends on the singular values. As shown in Fig. 1, N_{DoF} useful singular values of the near-field channel are almost equal. Therefore, the power allocation can be approximated as $\frac{1}{N_{\text{RF}}}\mathbf{I}_{N_{\text{RF}}}$, i.e. $\Sigma_i = \mathbf{I}_{N_r} + \frac{1}{N_{\text{RF}}\sigma_n^2}\mathbf{H}\mathbf{F}_i\mathbf{F}_i^H\mathbf{H}^H$.

Then, the SE of BM characterized by the mutual information can be written as

$$\begin{aligned}\mathcal{R}(\mathbf{p}) &= \mathcal{H}(\mathbf{y}) - \mathcal{H}(\mathbf{y}|\mathbf{F}_i, \mathbf{s}) \\ &= \mathbb{E}[-\log_2 f(\mathbf{y})] - \mathcal{H}(\mathbf{n}) \\ &= \int_{\mathbb{C}^{N_r}} f(\mathbf{y}) \log_2 f(\mathbf{y}) d\mathbf{y} - N_r \log_2(\pi e),\end{aligned}\quad (5)$$

where $\mathbf{p} = [p_1, p_2, \dots, p_K]^T$, $\mathcal{H}(\cdot)$ represents the entropy function and $\mathbb{E}[\cdot]$ denotes the expectation.

We aim to maximize the SE, which can be formulated as

$$\max_{\sum_{i=1}^K p_i=1} \mathcal{R}(\mathbf{p}). \quad (6)$$

It is hard to solve this problem directly due to the integration of complex functions. Fortunately, the upper bound (UB) for the entropy of GMM random vector \mathbf{y} has been established in [14], which is of the form

$$\mathcal{H}(\mathbf{y}) \leq \sum_{i=1}^K p_i (-\log p_i + \log [(\pi e)^{N_r} \det(\Sigma_i)]). \quad (7)$$

Combining (5) and (7), the UB of $\mathcal{R}(\mathbf{p})$ can be derived as

$$\mathcal{R}(\mathbf{p}) \leq \tilde{\mathcal{R}}(\mathbf{p}) = \sum_{i=1}^K p_i [\log_2 \det(\Sigma_i) - \log_2 p_i]. \quad (8)$$

In [15], it has been proved that the UB in (8) is tight in high signal-to-noise ratio (SNR) regions. Therefore, we replace $\mathcal{R}(\mathbf{p})$ in Eq. (6) with $\tilde{\mathcal{R}}(\mathbf{p})$, reconstructing the optimization problem as

$$\max_{\sum_{i=1}^K p_i=1} \sum_{i=1}^K p_i [\log_2 \det(\Sigma_i) - \log_2 p_i]. \quad (9)$$

Remark 2: The UB in (9) is tight in the high SNR regime, which implies that optimizing the original problem in (6) is equivalent to optimizing the UB in the high SNR region. However, it cannot guarantee tightness at low SNR. To fully illustrate the effectiveness, we have additionally included an optimization of the lower bound (LB) from (5). As proven in [16], this LB, with an added a constant gap of $N_r(\log e - 1)$, is tight in both the low and high SNR regimes. Therefore, optimizing this LB theoretically ensures optimality across the entire SNR range. The specific method is briefly explained in Appendix A, and simulation results are provided in Section IV for validation.

B. Optimization of Beam-space Activation Probability \mathbf{p}

The optimization problem (9) can be solved using the Lagrange multiplier method. The Lagrange multiplier for (9) can be formulated as

$$\mathcal{L}(\mathbf{p}, \lambda) = \sum_{i=1}^K p_i [\log_2 \det(\Sigma_i) - \log_2 p_i] - \lambda \left(\sum_{i=1}^K p_i - 1 \right). \quad (10)$$

The solution is obtained by solving

$$\begin{cases} \nabla_{p_i} \mathcal{L}(\mathbf{p}, \lambda) = \log_2 \det(\Sigma_i) - \log_2 p_i - \frac{1}{\ln 2} - \lambda = 0 \\ \nabla_{\lambda} \mathcal{L}(\mathbf{p}, \lambda) = \sum_{i=1}^K p_i - 1 = 0 \end{cases}, \quad (11)$$

where $\nabla_x f$ represents the derivation of f respect to x . Then, the optimal activation probability can be derived as

$$p_i^* = \frac{\det(\Sigma_i)}{\sum_{i=1}^K \det(\Sigma_i)}, \quad i = 1, 2, \dots, K. \quad (12)$$

Substituting (12) into (9), we obtain the asymptotic SE of BM

$$\begin{aligned}\mathcal{R}_{\text{BM}}^A &= \sum_{i=1}^K p_i^* [\log_2 \det(\Sigma_i) - \log_2 p_i^*] \\ &= \sum_{i=1}^K p_i^* \log_2 \left[\sum_{i=1}^K \det(\Sigma_i) \right] = \log_2 \left[\sum_{i=1}^K \det(\Sigma_i) \right].\end{aligned}\quad (13)$$

Moreover, the SE of the traditional scheme using the best beamspace transmission (BBT) can be expressed as³

$$\mathcal{C}_{\text{BBT}} = \log_2 \left[\max_{i=1, \dots, K} \det(\Sigma_i) \right]. \quad (14)$$

Remark 3: The complexity of the optimization of activation probability based on UB mainly comes from the K calculations of matrix determinant $\det(\Sigma_i)$, which is $\mathcal{O}(KN_r^3)$.

C. Optimization of the Number of Activated RF Chains N_{RF}^T

The number of activated RF chains directly affects the beamformer set \mathcal{F} and consequently impacts the performance of BM. Thus, optimizing N_{RF}^T is necessary for ensuring the performance superiority of BM.

The singular value decomposition (SVD) of \mathbf{H} is defined as $\mathbf{H} = \mathbf{U}\mathbf{S}\mathbf{V}^H$. Denote that the N_{DoF} largest singular values of \mathbf{H} are expressed as $\{\rho_1, \rho_2, \dots, \rho_{N_{\text{DoF}}}\}$. Then we can have

$$\mathbf{H}\mathbf{F}_i\mathbf{F}_i^H\mathbf{H}^H = \mathbf{U}_i \begin{bmatrix} (\rho_1^i)^2 & & \\ & \ddots & \\ & & (\rho_{N_{\text{RF}}^T}^i)^2 \end{bmatrix} \mathbf{U}_i^H, \quad (15)$$

where $\rho_j^i, j = 1, \dots, N_{\text{RF}}^T$ denotes the j -th singular value corresponding to the activated \mathbf{F}_i , \mathbf{U}_i denotes the left singular vectors corresponding to the singular values. According to the property of determinant $\det(\mathbf{I} + \mathbf{A}\mathbf{B}) = \det(\mathbf{I} + \mathbf{B}\mathbf{A})$, we have

$$\begin{aligned}\det(\Sigma_i) &= \prod_{j=1}^{N_{\text{RF}}^T} \left(1 + \frac{1}{N_{\text{RF}}^T \sigma_n^2} (\rho_j^i)^2 \right) \\ &\stackrel{(a)}{\approx} \left(1 + \frac{\|\mathbf{H}\|_F^2}{\sigma_n^2 N_{\text{RF}}^T N_{\text{DoF}}} \right)^{N_{\text{RF}}^T},\end{aligned}\quad (16)$$

where approximation (a) is obtained by assuming that the first N_{DoF} sub-channels occupy the main power of all sub-channels and N_{DoF} useful singular values are almost equal.⁴ According

³BBT uses beams formed by the right singular vectors corresponding to the N_{RF}^T largest channel singular values for transmission [7], [8].

⁴This means that $\sum_{i=1}^{N_{\text{DoF}}} \rho_i^2 \approx \|\mathbf{H}\|_F^2$.

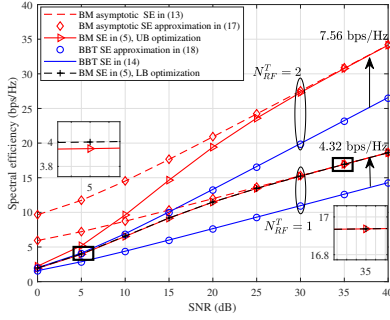


Fig. 3. The comparison of SE among different schemes over different SNRs.

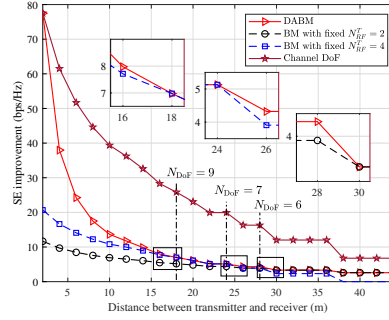


Fig. 4. SE improvement by DABM varies with distance at an SNR of 30 dB.

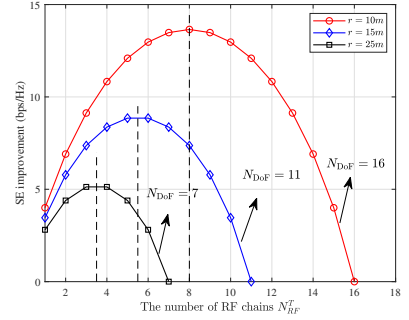


Fig. 5. SE improvement by DABM varies with the number of RF chains at an SNR of 30 dB.

to Fig. 1, the above assumptions are reasonable. Consequently, the asymptotic SE of BM can be approximated as

$$\mathcal{R}_{\text{BM}}^A \stackrel{(a)}{\approx} \log_2 \left[\binom{N_{\text{DoF}}}{N_{\text{RF}}^T} \left(1 + \frac{\|\mathbf{H}\|_F^2}{\sigma_n^2 N_{\text{RF}}^T N_{\text{DoF}}} \right)^{N_{\text{RF}}^T} \right]. \quad (17)$$

Accordingly, when the assumptions in (16) hold, the SE of BBT can be approximated as

$$\mathcal{R}_{\text{BBT}} \stackrel{(a)}{\approx} \log_2 \left[\left(1 + \frac{\|\mathbf{H}\|_F^2}{\sigma_n^2 N_{\text{RF}}^T N_{\text{DoF}}} \right)^{N_{\text{RF}}^T} \right]. \quad (18)$$

We use the SE improvement brought by BM as the evaluation metric, which can be denoted as

$$g = \mathcal{R}_{\text{BM}}^A - \mathcal{R}_{\text{BBT}} \approx \log_2 \left(\frac{N_{\text{DoF}}}{N_{\text{RF}}^T} \right). \quad (19)$$

Then, the solution for maximizing combination number $\left(\frac{N_{\text{DoF}}}{N_{\text{RF}}^T} \right)$ can be calculated as [17]

$$N_{\text{RF}}^T = \begin{cases} \frac{N_{\text{DoF}}-1}{2} \text{ or } \frac{N_{\text{DoF}}+1}{2}, & \text{if } N_{\text{DoF}} \text{ is odd} \\ \frac{N_{\text{DoF}}}{2}, & \text{if } N_{\text{DoF}} \text{ is even} \end{cases}. \quad (20)$$

This indicates that the SE improvement brought by BM is maximized when the number of RF chains is kept around $\frac{N_{\text{DoF}}}{2}$.

Through the above analysis, the relationship between the spatial DoFs and the number of RF chains is obtained for maximum SE improvement. As the distance r between the transmitter and receiver changes, the spatial DoFs vary. By dynamically adjusting the switch circuit in Fig. 2 to keep the number of activated RF chains around $\frac{N_{\text{DoF}}}{2}$, BM consistently maintains the maximum SE improvement.

IV. SIMULATIONS AND DISCUSSIONS

In the simulations, the carrier frequency is set to be 30 GHz, and the transceivers are equipped with half-wavelength spaced parallel 256-antenna ULA.

Fig. 3 shows the spectral efficiency of BM at the SNR from 0 dB to 40 dB. The distance between the transmitter and receiver is set to 8 meters, corresponding to $N_{\text{DoF}} = 20$. The real achieved SE in Eq. (5) is evaluated by utilizing Monte Carlo simulations to compute the expectation. Fig. 3 illustrates that the asymptotic SE in Eq. (13) exceeds the actual

SE at low SNR but perfectly coincides with it at high SNR, demonstrating the correctness of the asymptotic SE and the tightness of the UB at high SNR. Additionally, we simulate the LB optimization scheme when $N_{\text{RF}}^T = 1$ for comparison, as indicated by the black dashed line in Fig. 3. It can be observed that at low SNR, the LB optimization slightly outperforms the UB optimization by approximately 0.05 bps/Hz, while both are identical at high SNR regions. This is because the LB is tight at both high and low SNRs, whereas the UB is only tight at high SNRs, which has been discussed in Remark 2. However, the LB optimization has significantly high complexity, whereas the UB optimization achieves a solution with much lower complexity, with only negligible performance loss at low SNRs. Therefore, UB optimization is more suitable for practical applications. Meanwhile, the asymptotic SE approximation in Eq. (17) almost coincides with the asymptotic SE in Eq. (13), confirming the accuracy of the approximation. Similarly, the approximation in Eq. (18) is validated to be correct. Additionally, we have plotted the results for $N_{\text{RF}}^T = 1$ and $N_{\text{RF}}^T = 2$. It can be observed that the spectral efficiency improvement of BM changes from 4.32 bps/Hz to 7.56 bps/Hz, corresponding to $\log_2 \left(\frac{N_{\text{DoF}}}{1} \right)$ to $\log_2 \left(\frac{N_{\text{DoF}}}{2} \right)$. The correctness of Eq. (19) is further verified.

The detailed variation of the SE improvement brought by DABM along with the decrease in distance between the transmitter and receiver is shown in Fig. 4⁵. Both BBT and BM maintain the same number of RF chains. When N_{RF}^T is related to the distance, BBT becomes DAP as described in [8]. The SE improvement is quantified by comparing the SE of BM to that of BBT. As the distance decreases and the DoFs increase, the SE improvement is more significant for all curves. Obviously, compared to BM with a fixed number of RF chains, DABM achieves the maximum SE improvement. When N_{RF}^T satisfies Eq. (20), BM with fixed number of RF chains can reach the maximum SE improvement.

The impact of the number of RF chains on the SE improvement of BM is investigated in Fig. 5. Obviously, when the number of RF chains is around $\frac{N_{\text{DoF}}}{2}$, the SE improvement is maximized, intuitively proving the correctness of Eq. (19). When $N_{\text{RF}}^T = N_{\text{DoF}}$, BM degrades to BBT. This indicates that

⁵To focus on the impact of DoFs, we ignore the large-scale fading caused by distance, i.e., $\|\mathbf{H}\|_F^2$ remains constant with distance variation.

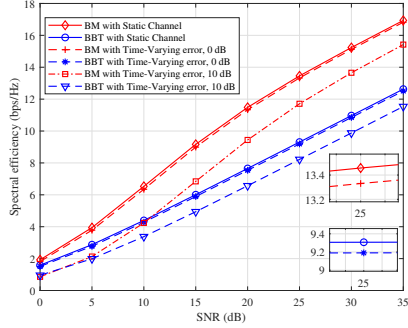


Fig. 6. The SE with time-varying channel caused by fast fading.

BBT is the optimal scheme when the sufficient RF chains are available. However, when the number of RF chains is limited ($N_{\text{RF}}^T < N_{\text{DoF}}$), BM enhances the near-field SE. The maximum SE improvement is achieved when (20) is satisfied. Thus, by using switch circuit to flexibly activate RF chains according to (20), DABM can obtain the maximum SE gain.

To evaluate the impact of time-varying channels caused by fast fading, we model the time-varying channel as an error model: $\mathbf{H} = \mathbf{H}_s + \mathbf{H}_t$, where \mathbf{H}_s represents the static part, and \mathbf{H}_t represents the time-varying part. The extent of channel variation due to fast fading is represented by $\frac{\|\mathbf{H}_t\|_F^2}{\|\mathbf{H}_s\|_F^2}$. In Fig. 6, it can be observed that time-varying channels cause performance degradation for both BM and BBT schemes, but BM still outperforms the BBT scheme, indicating that the BM scheme remains effective under similar channel conditions.

V. CONCLUSION

In this letter, we proposed the DABM scheme to enhance the SE in the near-field. We analyzed the SE of BM and derived a more concise UB on SE. The relationship between the SE improvement and the number of RF chains has been established. Also, a closed-form solution has been derived, indicating that the number of RF chains should be around $\frac{N_{\text{DoF}}}{2}$ for maximum SE improvement. Simulation results validate the correctness of the analysis and show that BM achieves the performance improvement when the number of RF chains is limited. Moreover, the proposed DABM offers the optimal performance gains as the distance varies. Our future research will focus on codebook-based BM to reduce the dependence on channel estimation.

APPENDIX A

SE LOWER BOUND OF $\mathcal{R}(\mathbf{p})$ OPTIMIZATION

According to Theorem 1 in [16] or the Proposition 1 in [18], the LB of SE in (5) is given as follows

$$\mathcal{R}^L(\mathbf{p}) = - \sum_{i=1}^{|\mathcal{F}|} p_i \log \left(\sum_{j=1}^{|\mathcal{F}|} \frac{p_j}{|\det(\boldsymbol{\Sigma}_i + \boldsymbol{\Sigma}_j)|} \right) - N_r \log e. \quad (21)$$

Furthermore, the LB adding a constant gap $N_r(\log e - 1)$ is proved to be tight in both the low and high SNR regime by Proposition 1 in [16]. Then the optimization of exact SE $\mathcal{R}(\mathbf{p})$

can be transferred into the optimization of $\mathcal{R}^L(\mathbf{p})$, which can be written as

$$\max_{\mathbf{p}} \mathcal{R}^L(\mathbf{p}) \quad \text{subject to} \quad \sum_{i=1}^K p_i = 1, p_i \geq 0. \quad (22)$$

Since the expression of LB is still too complicated, it is difficult to obtain a closed-form solution. It can be solved by a numerical optimization approach. Specifically, the [18] provides a gradient descent algorithm, which we employ to solve the LB optimization problem. The complexity of the gradient descent algorithm is $\mathcal{O}(N_{\text{iter}} K^3 N_r^3)$, which is much higher than that of UB optimization $\mathcal{O}(K N_r^3)$.

REFERENCES

- [1] A. Elzanaty, J. Liu, A. Guerra, F. Guidi, Y. Ma, and R. Tafazolli, "Near and far field model mismatch: Implications on 6G communications, localization, and sensing," *ArXiv*, vol. abs/2310.06604, 2023.
- [2] K. Qu, S. Guo, J. Ye, and H. Zhao, "Two-stage beamspace music-based near-field channel estimation for hybrid XL-MIMO," *IEEE Commun. Lett.*, vol. 28, no. 8, pp. 1949–1953, Aug. 2024.
- [3] M. Cui, Z. Wu, Y. Lu, X. Wei, and L. Dai, "Near-field MIMO communications for 6G: Fundamentals, challenges, potentials, and future directions," *IEEE Commun. Mag.*, vol. 61, no. 1, pp. 40–46, Jan. 2023.
- [4] Z. Wu and L. Dai, "Multiple access for near-field communications: SDMA or LDMA?" *IEEE J. Sel. Areas Commun.*, vol. 41, no. 6, pp. 1918–1935, June 2023.
- [5] H. Lu and Y. Zeng, "Near-field modeling and performance analysis for multi-user extremely large-scale MIMO communication," *IEEE Commun. Lett.*, vol. 26, no. 2, pp. 277–281, Feb. 2022.
- [6] Z. Xie, Y. Liu, J. Xu, X. Wu, and A. Nallanathan, "Performance analysis for near-field MIMO: Discrete and continuous aperture antennas," *IEEE Wireless Commun. Lett.*, vol. 12, no. 12, pp. 2258–2262, Dec. 2023.
- [7] X. Yu, J.-C. Shen, J. Zhang, and K. B. Letaief, "Alternating minimization algorithms for hybrid precoding in millimeter wave MIMO systems," *IEEE J. Sel. Topics Signal Process.*, vol. 10, no. 3, pp. 485–500, Apr. 2016.
- [8] Z. Wu, M. Cui, Z. Zhang, and L. Dai, "Distance-aware precoding for near-field capacity improvement in XL-MIMO," in *2022 IEEE 95th Vehicular Technology Conference (VTC2022-Spring)*. Helsinki, Finland: IEEE, June. 2022, pp. 1–5.
- [9] S. Guo and K. Qu, "Beamspace modulation for near field capacity improvement in XL-MIMO communications," *IEEE Wireless Commun. Lett.*, vol. 12, no. 8, pp. 1434–1438, Aug. 2023.
- [10] S. Payami and F. Tufvesson, "Channel measurements and analysis for very large array systems at 2.6 GHz," in *2012 6th European Conference on Antennas and Propagation (EUCAP)*, 2012, pp. 433–437.
- [11] Z. Zhou, X. Gao, J. Fang, and Z. Chen, "Spherical wave channel and analysis for large linear array in los conditions," in *2015 IEEE Globecom Workshops (GC Wkshps)*, 2015, pp. 1–6.
- [12] D. A. and Miller, "Communicating with waves between volumes: evaluating orthogonal spatial channels and limits on coupling strengths," *Applied optics*, vol. 39, no. 11, pp. 1681–1699, Apr. 2000.
- [13] S. Sun, R. Li, C. Han, X. Liu, L. Xue, and M. Tao, "How to differentiate between near field and far field: Revisiting the rayleigh distance," 2024. [Online]. Available: <https://arxiv.org/abs/2309.13238>
- [14] A. A. I. Ibrahim, T. Kim, and D. J. Love, "On the achievable rate of generalized spatial modulation using multiplexing under a Gaussian mixture model," *IEEE Trans. Commun.*, vol. 64, no. 4, pp. 1588–1599, Apr. 2016.
- [15] S. Guo, H. Zhang, and M.-S. Alouini, "Asymptotic capacity for MIMO communications with insufficient radio frequency chains," *IEEE Trans. Commun.*, vol. 68, no. 7, pp. 4190–4201, July 2020.
- [16] L. He, J. Wang, and J. Song, "Spatial modulation for more spatial multiplexing: RF-chain-limited generalized spatial modulation aided MM-Wave MIMO with hybrid precoding," *IEEE Trans. Commun.*, vol. 66, no. 3, pp. 986–998, Mar. 2018.
- [17] S. T. Smith, "The binomial coefficient $\binom{n}{x}$ for arbitrary x ," *Online J. Anal. Comb.*, vol. 15, 2020.
- [18] S. Guo, H. Zhang, P. Zhang, P. Zhao, L. Wang, and M.-S. Alouini, "Generalized beamspace modulation using multiplexing: A breakthrough in mmWave MIMO," *IEEE J. Sel. Areas Commun.*, vol. 37, no. 9, pp. 2014–2028, Sep. 2019.